J Nanopart Res (2014) 16:2389
DOI 10.1007/s11051-014-2389-z

RESEARCH PAPER

# White-light-controlled resistance switching in $TiO_2/\alpha$-$Fe_2O_3$ composite nanorods array

B. Sun · Q. L. Li · W. X. Zhao · H. W. Li ·
L. J. Wei · P. Chen

Received: 1 January 2014 / Accepted: 26 March 2014 / Published online: 11 April 2014


**Abstract** White-light-controlled resistance switching in $TiO_2/\alpha$-$Fe_2O_3$ composite nanorods array grown on fluorine-doped tin oxide substrate by hydrothermal process is investigated. The average length of $TiO_2/\alpha$-$Fe_2O_3$ nanorods is about 3.5 μm, and the average diameter is about 250 nm. The sizes of the α-$Fe_2O_3$ particles are in the range of 30 $\sim$ 70 nm. The current–voltage characteristics of the composite nanorods array show a good rectifying property and bipolar resistive-switching behavior, and the resistive-switching behavior can be regulated by white-light illumination at room temperature. This study is helpful for exploring the multifunctional materials and their applications in nonvolatile multistate memory devices.

**Keywords** $TiO_2/\alpha$-$Fe_2O_3$ composite nanorods array · White-light-controlled · Resistance switching · Nanocomposites

B. Sun · W. X. Zhao · H. W. Li · L. J. Wei ·
P. Chen (✉)
School of Physics Science and Technology, Southwest University, Chongqing 400715, China
e-mail: pchen@swu.edu.cn

B. Sun · W. X. Zhao
Institute for Clean Energy & Advanced Materials (ICEAM), Southwest University, Chongqing 400715, China

Q. L. Li
The Southwest University Hospital, Southwest University, Chongqing 400715, China

## Introduction

It is undeniable that resistance switching is one of the most promising candidates for the next generation of nonvolatile computer memories, which has high operational speed, high storage density, and low power consumption (Meijer 2008). Currently, a large variety of solid-state materials exhibit the resistance switching effect, including organic materials (Stewart et al. 2004; Ma et al. 2003), binary oxides (Liu et al. 2009; Schindler et al. 2009), amorphous Si (Jo et al. 2009), carbon-based materials (Li et al. 2008; Zhuge et al. 2010; He et al. 2009), and complex perovskite oxides such as $Pr_{1-x}Ca_xMnO_3$ (Liu et al. 2000), $La_{1-x}Ca_xMnO_3$ (Hasan et al. 2008), and $La_2CuO_{4+x}$ (Hamaguchi et al. 2006). Recently, a light-controlled resistance switching was observed in $Pd/Al_2O_3/SiO_2$ film and ZnO nanorod (Ungureanu et al. 2012; Park et al. 2012, 2013; Bera et al. 2013), which are added to the light as extra control parameter for the resistance switching. The light-controlled resistance switching provides the potential for non-volatile light-controlled memory applications.

In recent years, α-$Fe_2O_3$ has received increasing attention due to their extensive applications as magnetic materials, catalysts, pigments, gas sensors, optical and electromagnetic devices, drug delivery, tissue repairing engineering, and electromagnetic devices. α-$Fe_2O_3$ nanostructures with various morphologies have been successfully synthesized (Bean and Livingston 1959; Faust et al. 1989; Hyeon 2003;

Chen et al. 2005), and among these structures, one-dimensional $\alpha$-$Fe_2O_3$ possesses interesting physical properties, such as good light-harvesting and charge transport properties, and $\alpha$-$Fe_2O_3$ with band gap of 1.9–2.2 eV, which could absorb most of visible light, is a semiconductor material (Khan and Akikusa 1999; Beermann et al. 2002). At the same time, semiconductor-based photocatalysis has attracted extensive interest for basic and applied chemical utilization of solar energy (Burschka et al. 2013; Crossland Edward et al. 2013; Hodes 2013; Mitchinson 2008; Gratzel 2003), and one of the most commonly used materials is anatase $TiO_2$ (band gap 3.1–3.2 eV) (Adachi et al. 2012; Wu et al. 2011; Cao et al. 2011). Rutile $TiO_2$ has been proven to be comparable to anatase $TiO_2$ in dye-sensitized solar cells (DSSCs) with additional advantages in visible light including better chemical stability, photochemical activity, and higher refractive index (Liu and Aydil 2009; Diwald et al. 2004; Wang et al. 2007), and the rutile $TiO_2$ is a key material for water dissociation (Schaub et al. 2001). In addition, for the one-dimensional nature of $\alpha$-$Fe_2O_3$ and $TiO_2$, abundant availability, and the inexpensive and non-toxic nature of both the oxides make this composite material an exciting one for various applications (Liu and Gao 2006).

To the best of our knowledge, although the photocatalytic properties of individual $TiO_2$ have been intensively investigated (Jang et al. 2001; Beydoun and Amal 1999; Watson et al. 2004; Chu et al. 2008), the resistance switching characteristics of $TiO_2/Fe_2O_3$ composite materials have not yet been reported. In this paper, we present a white-light-controlled resistance switching behavior in $TiO_2/\alpha$-$Fe_2O_3$ composite nanorods array at room temperature.

## Experimental

### Preparation of $TiO_2/\alpha$-$Fe_2O_3$ composite nanorods array

$TiO_2/\alpha$-$Fe_2O_3$ composite nanorods array grown on the FTO substrate was prepared by hydrothermal process (Fig. 1a). All chemicals used in this work were of analytic reagent grade and commercially available, and used without further purification. We introduce the synthesis steps of the most preferred one in our experiments, and the detailed experimental procedures

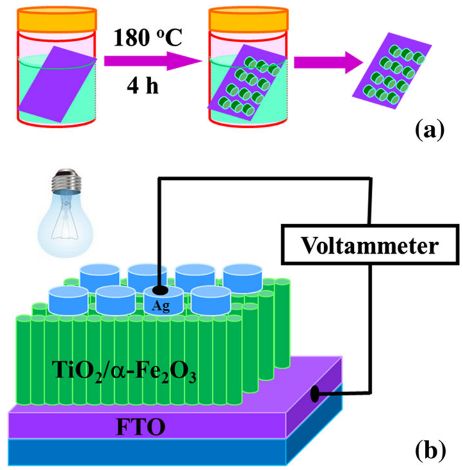


**Fig. 1** **a** The preparation process of $TiO_2/\alpha$-$Fe_2O_3$ composite nanorods grown on FTO substrate, **b** the experimental test circuit

are as follows: deionized water (7 mL) was mixed with hydrochloric acid (6.5 mL, 36.5–38 wt%) and stirred for 5 min; then, 0.2 mL titanium(IV) isopropoxide (TIP; 97 %, Sigma) (the TIP is liquid reagent) and 1.35 g $FeCl_3{\cdot}6H_2O$ (Sigma) were dissolved into the above solution and stirred for a few minutes; and then the mixture solution was transferred to a 50 mL Teflon-lined stainless steel autoclave. In addition, Fluorine-doped tin oxide (FTO)-coated glass substrates (NSG, 14 Ω per square) were cleaned prior to ultrasonic using acetone, ethanol, and deionized water, and subsequently dried in air. Then, the clean FTO substrate was put into the above mixture solution, and the conductive surface was down. The autoclave was put in an oven at a temperature of 180 °C for 4 h. After the autoclave was cooled to room temperature, the FTO substrate was rinsed with deionized water and subsequently annealed at 450 °C for 2.5 h in air.

### Characterization

Microstructure of $TiO_2/\alpha$-$Fe_2O_3$ composite nanorods was characterized by X-ray diffraction (XRD, Shimadzu XRD-7000 X-ray diffractometer) with Cu Kα radiation. Surface morphology of $TiO_2/\alpha$-$Fe_2O_3$ composite nanorods grown on FTO substrate was characterized using scanning electron microscopy (SEM, JSM-6510). The size, morphology, and the energy dispersive X-ray (EDX) analysis of the $TiO_2/\alpha$-$Fe_2O_3$ composite nanorods were observed by transmission electron microscopy (JEM-2100) at an acceleration voltage of 200 kV.

Figure 1b shows the schematic diagram of the test circuit. We used ordinary filament lamp with various power densities as light source, and the wavelength white-light is in the range of 400 $\sim$ 760 nm. Ag and FTO are top electrode and bottom electrode, respectively. The Ag electrodes with area about 4 $mm^2$ were prepared by silver glue. Electric characterizations were tested using the electrochemical workstation CHI-660D. The resistance switching properties of the samples were examined in the dark and under white-light illumination.

## Results and discussion

The crystalline compositions of the samples were characterized by XRD patterns. According to previous reports in the literature (Liu and Aydil 2009), the peak of FTO substrate is obvious. Therefore, in order to make diffraction peaks of $TiO_2/\alpha\text{-}Fe_2O_3$ clearer, we also present the XRD pattern of the pure FTO substrate without $TiO_2/\alpha\text{-}Fe_2O_3$ composite nanorods (Fig. 2a(A)). Figure 2a(B) shows the XRD pattern of $TiO_2/\alpha\text{-}Fe_2O_3$/FTO. We can see that the crystallizations of $TiO_2$ and $\alpha\text{-}Fe_2O_3$ are vary sufficiently without any other impurity phase. $TiO_2$ exhibits rutile phase. So, we can obtain a conclusion that the sample is $TiO_2/\alpha\text{-}Fe_2O_3$ composite nanorods. The composition of $TiO_2/\alpha\text{-}Fe_2O_3$ is further confirmed by elemental analysis carried out and observed from energy-dispersive X-ray spectra (EDS). The EDX data in Fig. 2b confirm that the elements of composition nanowire are Ti, Fe and O without any other impurities. The Fe/Ti ratio in the nanorod is about 30 %. We also prepared the $TiO_2/\alpha\text{-}Fe_2O_3$ nanorods array with other Fe/Ti ratio. But the white-light-regulated resistance switching for the $TiO_2/\alpha\text{-}Fe_2O_3$ nanorods array with other Fe/Ti ratio is not obvious. Therefore, we just report the results of the $TiO_2/\alpha\text{-}Fe_2O_3$ nanorods array with Fe/Ti ratio 30 %.

Figure 3a, b shows the SEM image of $TiO_2/\alpha\text{-}Fe_2O_3$ composite nanorods array grown on FTO substrate. We can see that the as-prepared sample consists of vertically and uniform nanorods (Fig. 3a). The typical cross-sectional SEM image of $TiO_2/\alpha\text{-}Fe_2O_3$ composite nanorods array is shown in Fig. 3b, which shows that the average length of $TiO_2/\alpha\text{-}Fe_2O_3$ nanorods is about 3.5 μm, and the diameter is about 250 nm (The inset to Fig. 3b). Figure 3c shows the TEM image of an individual $TiO_2/\alpha\text{-}Fe_2O_3$ composite nanorod, which shows that the nanorod is composed of $TiO_2$ and $\alpha\text{-}Fe_2O_3$, and $\alpha\text{-}Fe_2O_3$ is particle with diameter in the range of 30–70 nm. Figure 3d shows the high-resolution TEM (HRTEM) of $TiO_2/\alpha\text{-}Fe_2O_3$ composite nanorods. The fringes with a spacing of 0.33 nm correspond to (101) planes of $TiO_2$, and the fringes with a spacing of 0.3 nm correspond to (300) planes of $\alpha\text{-}Fe_2O_3$, and the inset shows the SAED pattern of the region without $\alpha\text{-}Fe_2O_3$ particles in Fig. 3c, which shows that the $TiO_2$ of $TiO_2/\alpha\text{-}Fe_2O_3$ composite nanorod is single-crystalline structure.

Figure 4a shows the current–voltage (I–V) curves of Ag/[$TiO_2/\alpha\text{-}Fe_2O_3$]/FTO in the dark and under

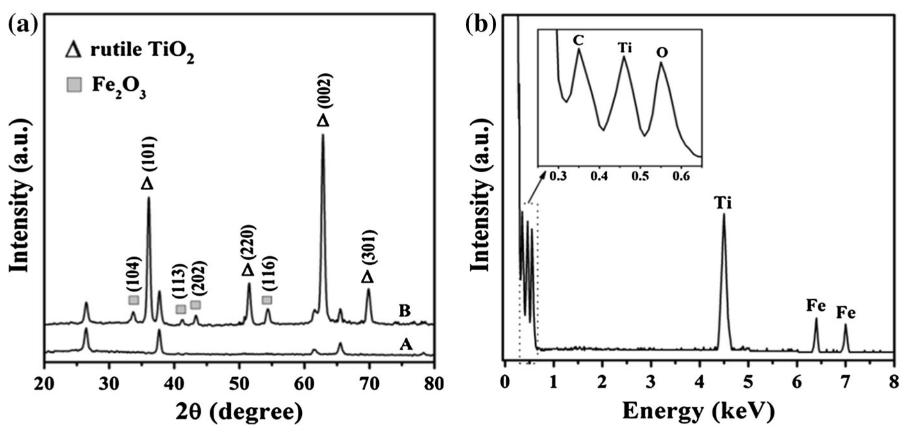


**Fig. 2** **a** *A* The XRD of the FTO substrate. *B* The XRD of $TiO_2/\alpha\text{-}Fe_2O_3$/FTO. **b** The EDX spectrum of $TiO_2/\alpha\text{-}Fe_2O_3$ composite nanorods, which shows the Fe/Ti ratio in the nanorods as 30 % nearly

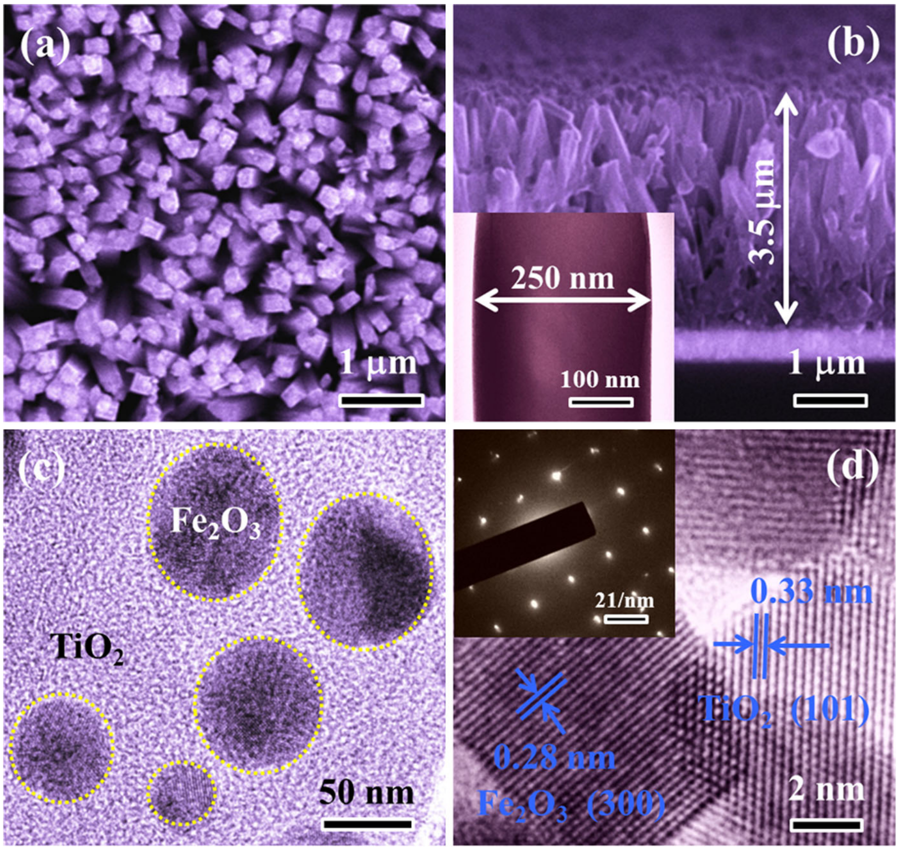


**Fig. 3** **a**, **b** Scanning electron microscopy (SEM) image of $TiO_2$/α-$Fe_2O_3$ composite nanorods grown on FTO substrate, the inset shows a single nanorod. **c** TEM image of individual $TiO_2$/α-$Fe_2O_3$ composite nanorod. **d** The HRTEM image of $TiO_2$/α-$Fe_2O_3$ composite nanorods. The fringes with a spacing of 0.33 nm correspond to (101) planes of $TiO_2$, and the fringes with a spacing of 0.28 nm correspond to (300) planes of α-$Fe_2O_3$. The *inset* is the corresponding SAED pattern

white-light illumination with various power densities at room temperature, which all exhibit asymmetric behavior with significant hysteresis. The arrows in the figure denote the sweeping direction of voltage. The asymmetric behavior of I–V curve demonstrates that a Schottky barrier is formed at the interface between $TiO_2$ and FTO, which was studied in previous work (Yang et al. 2014). The obvious bipolar resistive-switching behaviors are observed, which exhibit the rapid conversion and good reproducibility. The bipolar resistive-switching effect should result from the trapped and detrapped charge in the Schottky-like depletion layer (Ungureanu et al. 2012; Jang et al. 2006; Won et al. 2008; Jeong et al. 2007; Park et al. 2010). The inset of (Fig. 4a) shows a large resistance switching effects. The resistive-switching phenomenon becomes more obvious with the white-light power density increasing from 50 to 200 mW/cm$^2$. Therefore, the resistive-switching effect can be controlled by white-light with various power densities at room temperature, which demonstrates that $TiO_2$/α-$Fe_2O_3$ nanorod array is a potential candidate for multilevel light-controlled memory applications. It is elucidated that the resistance switching behavior is activated by the modulation of trapped electrons in the active layer under illumination conditions, as the total number of electrons is increased by joining the photogenerated current (Ungureanu et al. 2012; Park et al. 2012, 2013; Bera et al. 2013).

To evaluate the resistive-switching characteristics of $TiO_2$/α-$Fe_2O_3$ composite nanorods array, the resistance–time curves in the dark and under white-light illumination with a positive bias of 50 mV are tested and shown in Fig. 4b. It is obvious that the resistance is about 40 MΩ in the dark and 100 kΩ under white-light illumination with power density of 50 mW/cm$^2$,

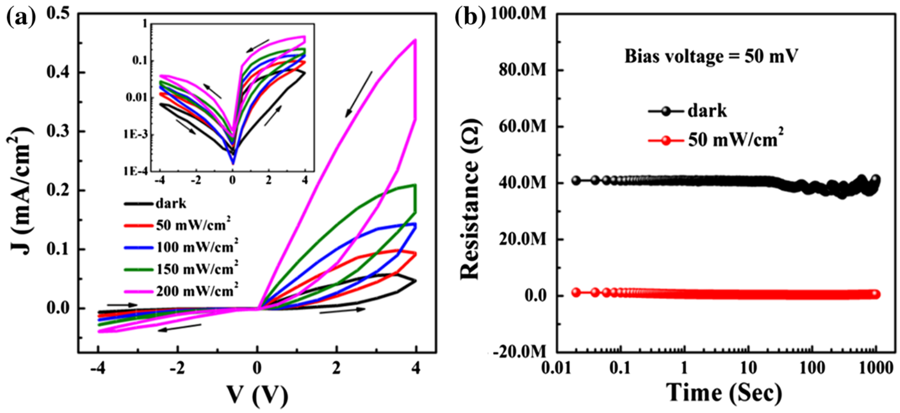


**Fig. 4** **a** Current–Voltage curves in the dark and under white-light illumination with various power density at room temperature. The *inset* is the resistance switching effects, **b** Resistance–Time curves in the dark and under white-light illumination

and the resistive-switching ratio is up to approximately three orders of magnitude. This adequately illustrates that the current density is greatly changed by white-light illumination. According to the above results, the steady light-controlled resistive-switching behavior in $TiO_2/\alpha\text{-}Fe_2O_3$ composite nanorods provides the potential for nonvolatile light-controlled memory applications.

## Conclusion

In this article, $TiO_2/\alpha\text{-}Fe_2O_3$ composite nanorods array with the resistance switching properties has been fabricated. These composite nanorods exhibit white-light-controlled resistance switching effect at room temperature. This work will shed light on the application of oxide composite materials in memory devices.

**Acknowledgments** This work was supported by the National Science Foundation of China (Grant No. 51372209).

## References

Adachi M et al (2012) Shape control of highly crystallized titania nanorods based on formation mechanism. J Mater Res 27(2):431–439. doi:10.1557/jmr.2011.353

Bean CP, Livingston JD (1959) The anisotropy of very small cobaltparticles. J Appl Phys 20(2–3):298–302. doi:10.1051/jphysrad:01959002002-3029800

Beermann N, Vayssieres L, Linquist ES, Hagfeldt A (2002) Synthesis of $Fe_2O_3/TiO_2$ nanorod–nanotube arrays by filling $TiO_2$ nanotubes with Fe. J Electrochem Soc 147(24):56–61. doi:10.1088/0957-4484/19/31/315601

Bera A, Peng H, Lourembam J, Shen Y, Sun XW, Wu T (2013) A versatile light-switchable nanorod memory: wurtzite ZnO on perovskite $SrTiO_3$. Adv Funct Mater 23:4977–4984. doi:10.1002/adfm.201300509

Beydoun D, Amal R, Low G, McEvoy S (1999) Role of nanoparticles in photocatalysis. J Nanopart Res 1(4):439–458. doi:10.1023/A:1010044830871

Burschka J et al (2013) Sequential deposition as a route to high-performance perovskite-sensitized solar cells. Nature 499:316. doi:10.1038/nature12340

Cao CB, Li JL, Wang X, Song XP, Sun ZQ (2011) Current characterization and growth mechanism of anodic titania nanotube arrays. J Mater Res 26:437. doi:10.1557/jmr.2010.33

Chen J, Xu L, Li WY, Gou X (2005) Alpha-$Fe_2O_3$ nanotubes in gas sensor and lithium-ion battery applications. Adv Mater 17(5):582–586. doi:10.1002/adma.200401101

Chu D, Yuan X, Qin G, Xu M, Zheng P, Lu J, Zha L (2008) Efficient carbon-doped nanostructured $TiO_2$ (anatase) film for photoelectrochemical solar cells. J Nanopart Res 10(2):357–363. doi:10.1007/s11051-007-9241-7

Crossland Edward JW et al (2013) Mesoporous $TiO_2$ single crystals delivering enhanced mobility and optoelectronic device performance. Nature 495:215–219. doi:10.1038/nature11936

Diwald O, Thompson TL, Zubkov T, Goralski EG, Walck SD, Yates JT Jr (2004) Photochemical activity of nitrogen-doped rutile TiO2 (110) in visible light. J Chem Phys 108:6004–6008. doi:10.1021/jp031267y

Faust BC, Hoffmann MR, Bahnemann DW (1989) Photocatalytic oxidation of sulfur-dioxide in aqueous suspensions of alpha-$Fe_2O_3$. J Chem Phys 93(17):6371–6381. doi:10.1021/j100354a021

Gratzel M (2003) Applied physics-solar cells to dye for. Nature 421:586–587. doi:10.1038/421586a

Hamaguchi M, Aoyama K, Asanuma S, Uesu Y, Katsufuji T (2006) Electric-field-induced resistance switching universally observed in transition-metal-oxide thin films. Appl Phys Lett 88(14):142508. doi:10.1063/1.2193328

Hasan M, Dong R, Choi HJ, Lee DS, Seong DJ, Pyun MB, Hwang H (2008) Uniform resistive switching with a thin reactive metal interface layer in metal-La(0.7)Ca(0.3)MnO(3)-metal

heterostructures. Appl Phys Lett 92(20):202102. doi:10.1063/1.2932148
He CL et al (2009) Nonvolatile resistive switching in graphene oxide thin films. Appl Phys Lett 95(23):232101. doi:10.1063/1.3271177
Hodes G (2013) Perovskite-based solar cells. Science 342:317–318. doi:10.1126/science.1245473
Hyeon T (2003) Chemical synthesis of magnetic nanoparticles. Chem Commun 8:927–934. doi:10.1039/b207789b
Jang HD, Kim S-K, Kim S-J (2001) Effect of particle size and phase composition of titanium dioxide nanoparticles on the photocatalytic properties. J Nanopart Res 3(2–3):141–147. doi:10.1023/A:1017948330363
Jang JS, Kim D, Seong TY (2006) Schottky barrier characteristics of Pt contacts to n-type InGaN. J Appl Phys 99(7):073704. doi:10.1063/1.2187274
Jeong DS, Schroeder H, Waser R (2007) Coexistence of bipolar and unipolar resistive switching behaviors in a Pt/$TiO_2$/Pt stack. Electrochem Solid-State Lett 10(8):G51–G53. doi:10.1149/1.2742989
Jo SH, Kim KH, Lu W (2009) Programmable resistance switching in nanoscale two-terminal devices. Nano Lett 9(1):496–500. doi:10.1021/nl803669s
Khan SUM, Akikusa J (1999) Efficient photochemical water splitting by a chemically modified n-$TiO_2$. J Chem Phys 103(718):4–9. doi:10.1126/science.1075035
Li YB, Sinitskii A, Tour JM (2008) Electronic two-terminal bistable graphitic memories. Nat Mater 7(12):966–971. doi:10.1038/nmat2331
Liu B, Aydil ES (2009) Growth of oriented single-crystalline rutile TiO2 nanorods on transparent conducting substrates for dye-sensitized solar cells. J Am Chem Soc 131:3985–3990. doi:10.1021/ja8078972
Liu H, Gao L (2006) Preparation and properties of nanocrystalline alpha-$Fe_2O_3$-sensitized $TiO_2$ nanosheets as a visible light photocatalyst. J Am Ceram Soc 89(1):370–373. doi:10.1111/j.1551-2916.2005.00686.x
Liu SQ, Wu NJ, Ignatiev A (2000) Electric-pulse-induced reversible resistance change effect in magnetoresistive films. Appl Phys Lett 76(19):2749–2751. doi:10.1063/1.126464
Liu M, Abid Z, Wang W, He XL, Liu Q, Guan WH (2009) Multilevel resistive switching with ionic and metallic filaments. Appl Phys Lett 94(23):233106. doi:10.1063/1.3151822
Ma LP, Pyo S, Ouyang J, Xu Q, Yang Y (2003) Nonvolatile electrical bistability of organic/metal-nanocluster/organic system. Appl Phys Lett 82(9):1419–1421. doi:10.1063/1.1556555
Meijer GI (2008) Materials science—who wins the nonvolatile memory race? Science 319:1625–1626. doi:10.1126/science.1153909
Mitchinson A (2008) Materials science—solar cells go round the bend. Nature 455:744. doi:10.1038/455744a
Park WY, Kim GH, Seok JY, Kim KM, Song SJ, Lee MH, Hwang CS (2010) A Pt/TiO2/Ti Schottky-type selection diode for alleviating the sneak current in resistance switching memory arrays. Nanotechnology 21(195201):4. doi:10.1088/0957-4484/21/19/195201
Park J, Lee S, Yong K (2012) Photo-stimulated resistive switching of ZnO nanorods. Nanotechnology 23:385707. doi:10.1088/0957-4484/23/38/385707
Park J, Lee S, Lee J, Yong K (2013) A light incident angle switchable ZnO nanorod memristor: reversible switching behavior between two non-volatile memory devices. Adv Mater 25:6423–6429. doi:10.1002/adma.201303017
Schaub R, Thostrup P, Lopez N, Lægsgaard E, Stensgaard I, Nørskov JK, Besenbacher F (2001) Oxygen vacancies as active sites for water dissociation on rutile $TiO_2$ (110). Phys Rev Lett 87(26):266104. doi:10.1103/PhysRevLett.87.266104
Schindler C, Staikov G, Waser R (2009) Electrode kinetics of Cu-$SiO_2$-based resistive switching cells: overcoming the voltage-time dilemma of electrochemical metallization memories. Appl Phys Lett 94(7):072109. doi:10.1063/1.3077310
Stewart DR, Chen Y, Willianms RS, Jeppesen JO, Nielsen KA, Stoddart F (2004) Molecule-independent electrical switching in Pt/organic monolayer/Ti devices Molecule-independent electrical switching in Pt/organic monolayer/Ti devices. Nano Lett 4(1):133–136. doi:10.1021/nl034795u
Ungureanu M, Zazpe R, Golmar F, Stoliar P, Llopis R, Casanova F, Hueso LE (2012) A light-controlled resistive switching memory. Adv Mater 24(18):2496–2500. doi:10.1002/adma.201200382
Wang Y, Zhang L, Deng K, Chen X, Zou Z (2007) Low temperature synthesis and photocatalytic activity of rutile $TiO_2$ nanorod superstructures. J Phys Chem C 111:2709–2714. doi:10.1021/jp066519k
Watson S, Beydoun D, Scott J, Amal R (2004) Preparation of nanosized crystalline $TiO_2$ particles at low temperature for photocatalysis. J Nanopart Res 6(2–3):193–207. doi:10.1023/B:NANO.0000034623.33083.71
Won S, Go S, Lee K, Lee J (2008) Resistive switching properties of Pt/TiO2/$n^+$-Si ReRAM for nonvolatile memory application. Electron Mater Lett 4(1):29–33
Wu JS et al (2011) Growth of rutile $TiO_2$ nanorods on anatase $TiO_2$ thin films on Si-based substrates. J Mater Res 26:1646. doi:10.1557/jmr.2011.190
Yang M, Ding B, Lee J-K (2014) Surface electrochemical properties of niobium-doped titanium dioxide nanorods and their effect on carrier collection efficiency of dye sensitized solar cells. J Power Sources 245:301–307. doi:10.1016/j.jpowsour.2013.06.016
Zhuge F, Dai W, He CL, Wang AY, Liu YW, Li M, Wu YH, Cui P, Li RW (2010) Nonvolatile resistive switching memory based on amorphous carbon. Appl Phys Lett 96(16):163505. doi:10.1063/1.3406121